Influence of increased cell densities on product ratio and productivity in syngas fermentation

Lukas Perret,* Nikolaos Boukis, and Jörg Sauer

Institute of Catalysis Research and Technology, Karlsruhe Institute of Technology, 76344 Eggenstein-Leopoldshafen, Germany

E-mail: lukas.perret@kit.edu

Phone: +49 (0)721 608-22171. Fax: +49 (0)721 608-22244

Abstract

Synthesis gas fermentation with anaerobic microorganisms such as *C. ljungdahlii* enables highly selective conversion of substrate gases such as CO, CO_2 and H_2 to high value intermediates like organic acids and alcohols. By using a biomass retention system with the aid of cross-flow ultrafiltration in an external circuit for biomass retention at a CSTR, we have succeeded in retaining the biocatalyst in the reactor and in increasing the cell density by more than 160 % and the space-time yield of C_2 products by 46 %. In addition, we found that the use of a cell retention system promoted ethanol formation and decreased the acetic acid to ethanol product ratio. Low partial pressures of CO in the exhaust gas were found to promote hydrogen uptake and ethanol formation. The space-time yield of ethanol, $8.71\,\mathrm{mmol\,L^{-1}\,h^{-1}}$, is the highest yield measured to date with an unmodified strain of *C. ljungdahlii*.

Introduction

The possibility of using synthesis gas fermentation to convert hydrogen and carbonaceous gases such as CO and CO_2 into chemicals, fuels and other valuable products could be of great importance to a future circular economy.[1,2] The advantages of syngas fermentation over heterogeneous catalysis are low process pressures and process temperatures, self-regeneration of the biocatalyst, and complete gas conversion without the need for a recirculation loop.[3] H_2, CO and CO_2 can be obtained e.g. by (co-)electrolysis,[4,5] gasification of biomass,[6] from industrial waste gases[7] or air capture[8] and could be converted to $C_2 - C_8$ compounds by acetogenic bacteria.[9–12] Anaerobic acetogenic bacteria convert CO_2 to acetyl-CoA via the Wood-Ljungdahl pathway and they produce acetic acid and ethanol in a first process step.[13] Both H_2 and CO serve as reducing agents.[14,15] A major bottleneck for the commercialization of syngas fermentation is the low space-time yield, which is up to three orders of magnitude lower than of heterogeneous catalysis.[3] Due to low product concentrations, product separation and purification is associated with high costs. Therefore, an increase of the cell density, which means an increase of the density of the biocatalyst in the reactor, represents an essential key variable in order to increase the space-time yield as part of the process development.[3] By using a biomass retention system, the outflow of the biocatalyst in the product stream during continuous operation can be avoided and thus an increase in cell density can be achieved. Centrifugation, filtration, or solid/liquid separators can be used to retain biomass.[16] Higher cell densities and an increase of space-time yield through the use of a biomass retention system have already been demonstrated in numerous studies on acetogenic microorganisms, see de Medeiros et al.,[17] Kantzow et al.,[18] Richter et al.,[19] Gaddy et al.,[16] Phillips et al.,[20] Abubackar et al.,[21] Mayer et al.[22] and Molitor et al..[23] However, to the best of our knowledge, detailed studies on the influence of cell retention on syngas fermentation are missing: (1.) Is the space-time yield proportional to cell density? (2.) Does cell retention affect the product ratio? (3.) Does total cell retention lead to an accumulation of carbon in the reactor? In order to answer these questions, we are investigating the influence of total cell retention on syngas fermentation in continuous operation by switching the external circuit for biomass retention on or off as desired during experimental operation. Furthermore, the influence of increasing gas flow and nutrient medium supply on fermentation at high cell densities is investigated.

Material and methods

Microorganism, cultivation and nutrient medium

The anaerobic, acetogenic bacterium *Clostridium ljungdahlii* (DSM 13528) is used as the biocatalyst. The composition of the culture medium for pre-cultivation and process is adapted from the culture medium of Stoll et al.,[24] the components are: 20 g/L 2-(N-morpholino) ethanesulfonic acid (MES), 0.5 g/L yeast extract, 2 g/L NaCl, 0.33 g/L NH_4Cl, 0.25 g/L KCl, 0.25 g/L KH_2PO_4, 0.5 g/L $MgSO_4 \cdot 7H_2O$, 0.1 g/L $CaCl_2 \cdot 2H_2O$, 0.001 g/L resazurin and 10 ml solution each of vitamins and trace elements per liter of medium. The components of the vitamin solution are: 0.002 g/L biotin, 0.002 g/L folic acid, 0.01 g/L pyridoxine, 0.005 g/L thiamine-HCl, 0.005 g/L riboflavin, 0.005 g/L niacin, 0.005 g/L Ca-pantothenate, 0.005 g/L cobalamin, 0.005 g/L 4-aminobenzoic acid and 0.005 g/L liponic acid. The components of the trace element solution are: 2 g/L nitrilotriacetic acid, 1 g/L $MnSO_4 \cdot H_2O$, 0.567 g/L $FeSO_4 \cdot 7H_2O$, 0.2 g/L $CoCl_2 \cdot 6H_2O$, 0.2 g/L $ZnSO_4 \cdot 7H_2O$, 0.02 g/L $CuCl_2 \cdot 2H_2O$, 0.02 g/L $NiCl_2 \cdot 6H_2O$, 0.02 g/L $Na_2MoO_4 \cdot 2H_2O$, 0.02 g/L $Na_2SeO_3 \cdot 5H_2O$ and 0.022 g/L $Na_2WO_4 \cdot 2H_2O$. The pH of the culture medium is adjusted to the desired value of 5.9 by adding KOH pellets. The culture medium is first anaerobized by intensive sparkling with nitrogen and in a further step with a gas mixture of 80 vol.% N_2 and 20 vol.% CO_2 and then sterilized at 121 °C for 20 min. For pre-cultivation, 1 g/L cysteine-HCl $\cdot$ H_2O is sterilely injected into the culture medium, and 0.3 g/L for the experimental run. Pre-cultivation is performed strictly anaerobically in three steps at 37 °C as described in Stoll et al..[24]

Experimental setup

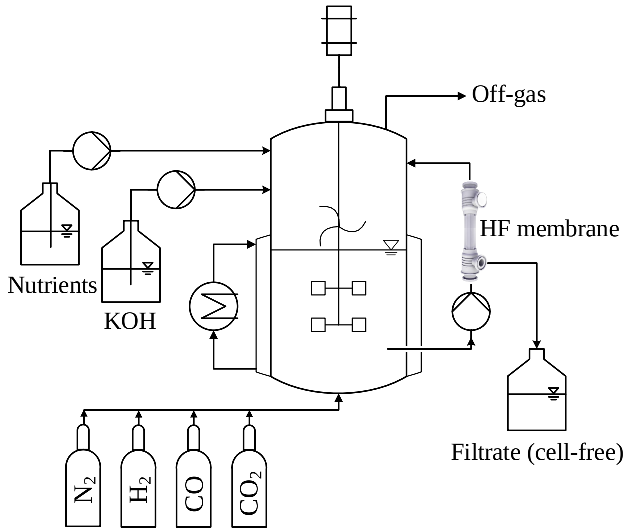

Figure 1: Experimental setup for a continuous fermentation including cross-flow filtration with a hollow fiber (HF) membrane (reference: repligen.com) in an external circle for biomass retention.

The experimental setup for continuous fermentation is shown in Fig. 1. The experimental unit includes a stainless steel CSTR (4 liter, inner diameter 126 mm) with double jacket and thermostat for temperature control, a gas mixing station (Bronkhorst, Netherlands) to adjust gas flow rate and gas composition of the four gases N_2, H_2, CO and CO_2, a syringe pump unit (CETONI, Germany) to deliver the nutrient medium, a HPLC pump (BISCHOFF, Germany) to deliver the base and a peristaltic pump (Albin Pump, France) for the external circuit of cross-flow filtration with a hollow fiber membrane (REPLIGEN, Netherlands, PES membrane, pore size 0.2 μm, specific surface 470 cm^2) for biomass retention during continuous operation. The gas inlet is at the bottom of the reactor via two gas frits (bbi-biotech, Germany, pore size 20 μm) and distributed via two six-bladed disk impellers (Buddeberg, Germany) mounted on the stirrer shaft. An impeller (C3 Prozess- und Analysentechnik, Germany, outer diameter 94 mm) for mechanical foam destruction is also located on the stirrer shaft above the filling level. Chemical additives for foam destruction are not used since they are expected to influence the gas-liquid mass transfer.[25] A high-pressure/high-temperature pH electrode (Walchem, USA) is located in the reactor connected to the HPLC pump to dose the base. Via a magnetic valve (RCT, Germany), fermentation broth can either be drained directly from the reactor or via the filtrate outlet at the hollow filter membrane; this allows the experimental plant to be operated even without the external circuit for biomass retention. A level probe in a communicating vessel (dead volume 270 ml, without aeration) is used to detect the level in the reactor and is linked to the magnetic valve to keep the level of the fermentation broth constant. The reactor with periphery is sterilized with 0.5 % peracetic acid and superheated steam (120-130 °C) just before the beginning of the experiment. Sterile filters (pore size 0.2 μm) in the gas supply pipe, in the feed supply pipe and in the exhaust gas prevent external contamination during operation of the experiment.

Process parameters

The measured data presented in this work were generated during two long-term experiments (experiment A: total process time of 1683 h and experiment B: total process time of 3097 h). For the evaluation, only measurement data from steady-state intervals were considered. Areas with steady state behavior are those areas in which gas uptake rates and productivities neither increase nor decrease continuously, but remain constant and fluctuate around an average value. The standard deviation in these areas is less than 10 %. The following parameters apply to all experiments: the temperature in the reactor is 37 $°C$, atmospheric pressure conditions are present and the reaction volume in the 4-liter reactor is 2.2 liters excluding the volumes of the circuits for level detection (269 ml) and biomass retention (126 ml). The specific energy input P/V_l into the CSTR through the stirrer (600 rpm) is 1.36 kW/m^3. The volume flow of the peristaltic pump in the external circuit for biomass retention is 10 L/h, the average residence time of the liquid phase in the external circuit is 45 seconds. In the external circuit for biomass retention, there is no external supply of substrate gas. Further process parameters can be taken from Tab. 1 and Tab. 2. For the composition of the substrate gas, it was ensured that hydrogen was present in excess for the stoichiometrically complete conversion of CO and CO_2 to ethanol. Slight differences in the gas composition between experiments A and B are based on further investigations, which are not part of this study.

Table 1: Experimental parameters of experiment A. The intervals $\overline{\mathrm{CR}}$, CR, $\mathrm{CR}_{\dot{V}_{\mathrm{G}\uparrow}}$ and $\mathrm{CR}_{\dot{V}_{\mathrm{G}\uparrow\uparrow}}$ represent steady-state areas from experiment A and differ in the selected experimental parameters. $\overline{\mathrm{CR}}$: the fermentation process is operated without a cell retention (CR) system. CR: fermentation process operated with a cell retention system. $\mathrm{CR}_{\dot{V}_{\mathrm{G}\uparrow}}$: increase of substrate gas flow while cell retention is still activated. $\mathrm{CR}_{\dot{V}_{\mathrm{G}\uparrow\uparrow}}$: second increase of substrate gas flow while cell retention is still activated.

	$\overline{\mathrm{CR}}$	CR	$\mathrm{CR}_{\dot{V}_{\mathrm{G}\uparrow}}$	$\mathrm{CR}_{\dot{V}_{\mathrm{G}\uparrow\uparrow}}$
Cell retention	✗	✓	✓	✓
$\dot{V}_{\mathrm{G}}$ / mL min^{-1}	$\longleftarrow$ 80 $\longrightarrow$		105	123
$H_2/CO/CO_2/N_2$ / vol. %	$\longleftarrow$ 48/16/4/32 $\longrightarrow$			61/20/5/14
$H_2 : CO : CO_2$	$\longleftarrow$ 70.5 : 23.5 : 6 $\longrightarrow$			
D / h^{-1}	$\longleftarrow$ 0.03 $\longrightarrow$			
τ / h	$\longleftarrow$ 33.3 $\longrightarrow$			
pH	$\longleftarrow$ 5.85 $\longrightarrow$			
duration of interval / h	52	55	31	129
number of gas samples	208	217	122	516
number of liquid samples	3	4	3	7

Table 2: Experimental parameters of experiment B. The intervals $\mathrm{CR}_{\mathrm{D}=0.03}$, $\mathrm{CR}_{\mathrm{D}=0.04}$, $\mathrm{CR}_{\mathrm{D}=0.05}$ and $\overline{\mathrm{CR}}_{\mathrm{B}}$ represent steady-state areas from experiment B and differ in the selected experimental parameters. The dilution rate D is increased from 0.03 h^{-1} ($\mathrm{CR}_{\mathrm{D}=0.03}$) to 0.04 h^{-1} ($\mathrm{CR}_{\mathrm{D}=0.04}$) to 0.05 h^{-1} ($\mathrm{CR}_{\mathrm{D}=0.05}$). Finally, cell retention is deactivated ($\overline{\mathrm{CR}}_{\mathrm{B}}$).

	$\mathrm{CR}_{\mathrm{D}=0.03}$	$\mathrm{CR}_{\mathrm{D}=0.04}$	$\mathrm{CR}_{\mathrm{D}=0.05}$	$\overline{\mathrm{CR}}_{\mathrm{B}}$
Cell retention	✓	✓	✓	✗
$\dot{V}_{\mathrm{G}}$ / mL min^{-1}	126	$\longleftarrow$ 111 $\longrightarrow$		62
$H_2/CO/CO_2/N_2$ / vol. %	65/18/7/9	65/18/7/11		59/16/7/19
$H_2 : CO : CO_2$ / %	$\longleftarrow$ 72 : 20 : 8 $\longrightarrow$			
D / h^{-1}	0.03	0.04	0.05	0.03
τ / h	33.3	25	20	33.3
pH	$\longleftarrow$ 5.9 $\longrightarrow$			
duration of interval / h	85	75	53	64
number of gas samples	406	360	253	306
number of liquid samples	4	4	3	3

Analytical methods

The composition of the exhaust gas is analyzed via a 2-channel micro gas chromatograph (INFICON, USA) every 15 minutes, the measurement time is three minutes, the carrier gases are argon and helium. Since gaseous nitrogen is not utilized by the bacteria, the volume fraction of nitrogen in the exhaust gas together with the supplied nitrogen volume flow through the substrate gas can be used to calculate the off-gas volume flow and the individual gas uptake rates, see Oswald et al..[26] A sample can be taken from the reactor via a valve for offline measurement of cell density, carbon content and product concentrations. Cell density is determined using a UV-VIS spectrometer (VWR, Germany) via optical density at a wavelength of 600 nm. For measured values $OD_{600} > 0.45$, samples are diluted with a NaCl solution (9 g/L) and the measurement is repeated. Cell separation is achieved by centrifugation at 12,000 g for 15 min. In the cell-free samples, the concentration of formic acid, acetic acid and ethanol is determined by HPLC using an Aminex HPX-87H column (Hitachi, Japan) and H_2SO_4 as eluent (4 mmol/L). The total organic carbon content TOC was determined by combustion catalytic oxidation and difference method TC-IC (DIMATEC, Germany).

Results

Influence of cell retention

The first experiment (experiment A interval $\overline{\mathrm{CR}}$) was performed without cell retention. The dilution rate was $0.03\,\mathrm{h}^{-1}$ and the resulted cell density $1.19\,\mathrm{g\,L}^{-1}$. By activating cell retention (experiment A interval CR), cell density increases by 160 % to $3.15\,\mathrm{g\,L}^{-1}$, see Fig. 2 E. Biomass-specific H_2 uptake decreases from $14.16\,\mathrm{mmol\,g}^{-1}\,\mathrm{h}^{-1}$ to $9.54\,\mathrm{mmol\,g}^{-1}\,\mathrm{h}^{-1}$, that of CO decreases from $10.96\,\mathrm{mmol\,g}^{-1}\,\mathrm{h}^{-1}$ by more than 50 % to $4.48\,\mathrm{mmol\,g}^{-1}\,\mathrm{h}^{-1}$, while q_{CO_2} increases from $0.14\,\mathrm{mmol\,g}^{-1}\,\mathrm{h}^{-1}$ to $1\,\mathrm{mmol\,g}^{-1}\,\mathrm{h}^{-1}$, see Fig. 2 A.

In contrast to the biomass-specific gas uptake rate, the gas uptake rate r increases for all three substrate gases: from $0.17\,\mathrm{mmol\,L^{-1}\,h^{-1}}$ to $3.17\,\mathrm{mmol\,L^{-1}\,h^{-1}}$ for CO_2, from $13.09\,\mathrm{mmol\,L^{-1}\,h^{-1}}$ to $14.14\,\mathrm{mmol\,L^{-1}\,h^{-1}}$ for CO and from $16.91\,\mathrm{mmol\,L^{-1}\,h^{-1}}$ to $30.09\,\mathrm{mmol\,L^{-1}\,h^{-1}}$ for H_2, see Fig. 2 B. As the gas volume flow is not changed in the interval CR, the increased gas uptake leads to an increase in gas conversions (see Tab. S1), resulting in a nearly complete conversion of CO with $X_{\mathrm{CO}}= 0.97$.

The biomass-specific formation of acetic acid and ethanol and their sum as C_2 components are shown in Fig. 2 C. By activating the biomass retention, the biomass-specific formation of acetic acid decreases from $3.73\,\mathrm{mmol\,g^{-1}\,h^{-1}}$ to $1.32\,\mathrm{mmol\,g^{-1}\,h^{-1}}$, while q_{EtOH} is not affected by cell retention ($1.60\,\mathrm{mmol\,g^{-1}\,h^{-1}}$ without cell retention and $1.63\,\mathrm{mmol\,g^{-1}\,h^{-1}}$ with cell retention). Due to the decreased acetic acid formation with cell retention, C_2 productivity decreases by 45 % from $5.33\,\mathrm{mmol\,g^{-1}\,h^{-1}}$ to $2.95\,\mathrm{mmol\,g^{-1}\,h^{-1}}$. However, as cell density increases by 160 %, there is still a 46 % increase of space-time yield of C_2 products during operation with cell retention ($9.31\,\mathrm{mmol\,L^{-1}\,h^{-1}}$ for CR compared to $6.36\,\mathrm{mmol\,L^{-1}\,h^{-1}}$ for $\overline{CR}$), see Fig. 2 D. This increase is a result entirely of the increased space-time yield of ethanol ($5.14\,\mathrm{mmol\,L^{-1}\,h^{-1}}$ for CR compared to $1.91\,\mathrm{mmol\,L^{-1}\,h^{-1}}$ for $\overline{CR}$). The space-time yield of acetic acid is not significantly affected by cell retention and takes a value of $4.45\,\mathrm{mmol\,L^{-1}\,h^{-1}}$ ($\overline{CR}$) and $4.17\,\mathrm{mmol\,L^{-1}\,h^{-1}}$ (CR), respectively. As the space-time yield of ethanol increases, the acetic acid to ethanol product ratio reverses, from 2.33 without cell retention ($\overline{CR}$) to 0.81 with cell retention (CR), see Fig. 2 F. This leads to a lower effort of neutralization of the C_2 product stream: the amount of potassium hydroxide decreases by more than 35 % from $0.7\,\mathrm{mmol_{KOH}\,mmol_{C_2}^{-1}}$ without cell retention to $0.45\,\mathrm{mmol_{KOH}\,mmol_{C_2}^{-1}}$ with cell retention, see Tab. S1.

This shift in the product ratio can be seen clearly in the selectivity in Fig. 3: without cell retention ($\overline{CR}$), two-thirds of the carbon uptake is converted to acetic acid, with cell retention (CR) it is 48 %, while 59 % is converted to ethanol. In addition, without biomass retention ($\overline{CR}$), cells are continuously washed out with the product stream, so 10 % of the

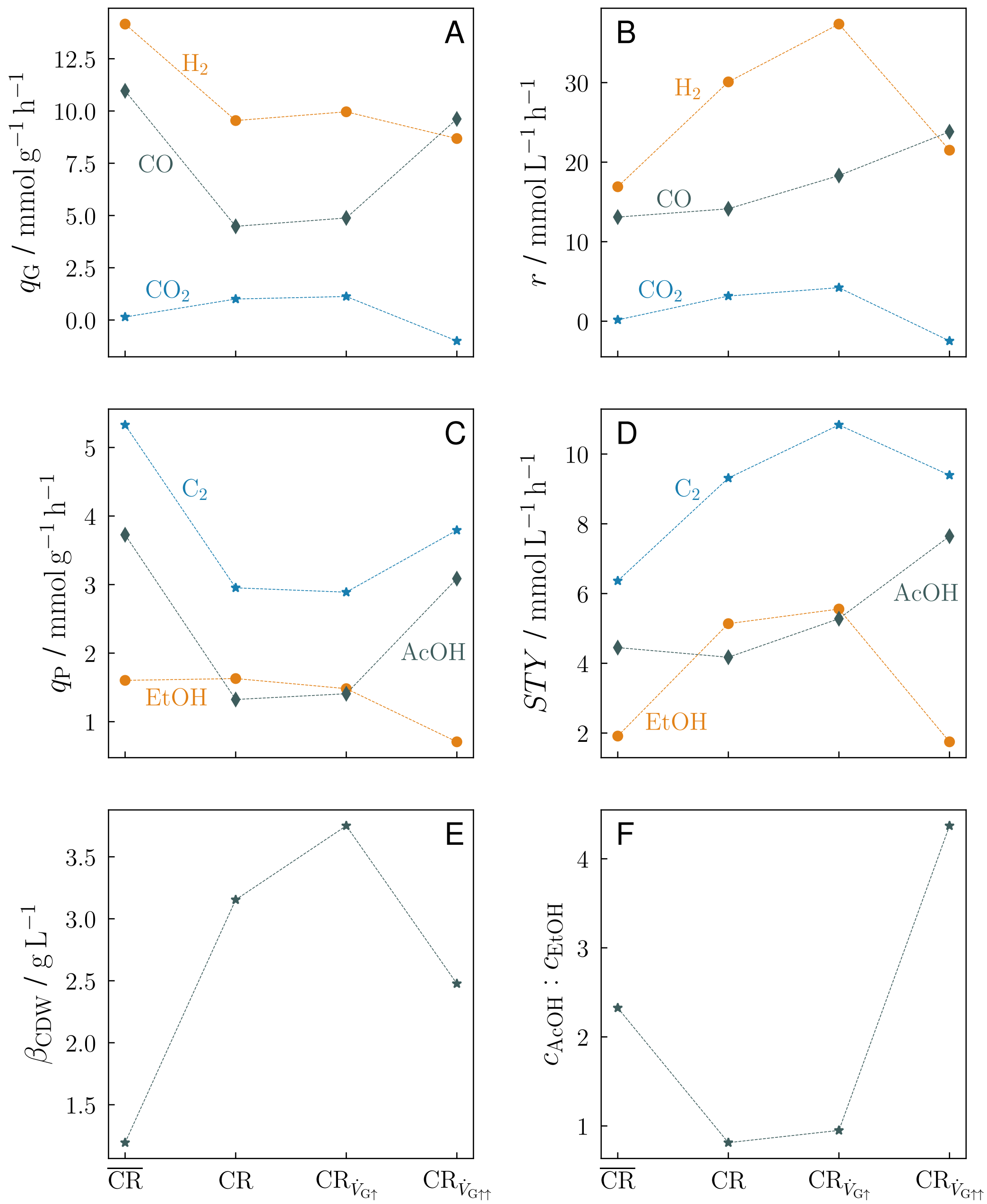

Figure 2: Influence of cell retention (CR) vs. no cell retention ($\overline{\mathrm{CR}}$) and increase of substrate gas with activated cell retention ($\mathrm{CR}_{\dot{V}_{\mathrm{G}\uparrow}}$, $\mathrm{CR}_{\dot{V}_{\mathrm{G}\uparrow\uparrow}}$). Averaged measured data of steady-state areas. A: biomass-specific gas consumption rate; B: gas consumption rate; C: biomass-specific productivity; D: space-time yield; E: concentration of cell dry weight; F: product ratio.

carbon uptake is used to continuously build up new biomass. With total cell retention (CR), a continuous build up of new biomass is not necessary, so the fraction for biomass is not required. Total selectivities greater than 100 % are presumably due to measurement inaccuracies, see also carbon balance in Tab. S1.

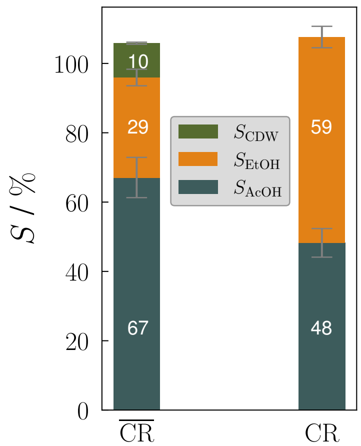

Figure 3: Carbon-based selectivity S with standard deviation averaged in the steady-state intervals $\overline{\mathrm{CR}}$ (without cell retention) and CR (cell retention activated).

Influence of an increased substrate gas flow with activated cell retention

As already shown, the activation of cell retention leads to an increase of the gas conversions (see Tab. S1 intervals $\overline{\mathrm{CR}}$ and CR). This leads to a nearly complete conversion of CO, resulting in CO_2 serving as the sole additional carbon source. To rule out the possibility that the increased space-time yield of ethanol and the shift in the product ratio are the results of these gas limitations and not a consequence of cell retention, the gas feed is increased in two steps to 105 mL min^{-1} (interval $\mathrm{CR}_{\dot{V}_{G\uparrow}}$) and finally to 123 mL min^{-1} (interval $\mathrm{CR}_{\dot{V}_{G\uparrow\uparrow}}$) with a constant ratio of $H_2 : CO : CO_2$.

Increasing the gas volume flow by 25 ml min^{-1}, corresponding to 31 %, leads to increased biomass-specific gas uptake: q_{H_2} increases by 4 % to 9.96 mmol g^{-1} h^{-1}, q_{CO} by 9 % to 4.88 mmol g^{-1} h^{-1} and q_{CO_2} by 13 % to 1.13 mmol g^{-1} h^{-1}, see Fig. 2 A. In addition, the increase in gas volume flow leads to an increase in cell density by 19 % to 3.75 g L^{-1} (see Fig. 2 E), so that the gas uptake rate r for all three gases increases significantly: r_{H_2} by 24 % to 37.36 mmol L^{-1} h^{-1}, r_{CO} by 29 % to 18.31 mmol L^{-1} h^{-1} and r_{CO_2} by 33 % to 4.22 mmol L^{-1} h^{-1}, see Fig. 2 B. The increase in the average gas uptake rate of all three substrate gases is 26 %, which is 5 percentage points below the increase in gas volume flow of 31 %. Biomass-specific ethanol formation decreases by 9 % to 1.48 mmol g^{-1} h^{-1}, while q_{EtOH} increases by 7 % to 1.41 mmol g^{-1} h^{-1}, see Fig. 2 C. In contrast to biomass-specific ethanol formation, there is an increase in the space-time yield of ethanol due to an increase in cell density: STY_{EtOH} increases by 8 % to 5.56 mmol L^{-1} h^{-1}, STY_{AcOH} increases by 27 % to 5.28 mmol L^{-1} h^{-1}, see Fig. 2 D. The increase in the gas flow leads to an overall increase of C_2 space-time yield by 16 % to 10.84 mmol L^{-1} h^{-1}. The product ratio of acetic acid to ethanol increases slightly, from 0.81 to 0.95, and is still significantly smaller compared to the product ratio of 2.33 without the operation of a cell retention system ($\overline{\mathrm{CR}}$), see Fig. 2 F.

The second increase in gas flow ($\mathrm{CR}_{\dot{V}_{G\uparrow\uparrow}}$) leads to a doubling of the biomass-specific gas uptake rate of CO to 9.62 mmol g^{-1} h^{-1} and to a reduction of q_{H_2} and q_{CO_2} by 13 % to 8.68 mmol g^{-1} h^{-1} and 88 % to -1.00 mmol g^{-1} h^{-1}, respectively, see Fig. 2 A. With that for the first time more CO_2 is formed than taken up by the microorganisms, responsible for this is the oxidation of CO to CO_2. In contrast to the first gas flow increase ($\mathrm{CR}_{\dot{V}_{G\uparrow}}$), there is no further increase in cell density, but a reduction of 34 % to 2.48 g L^{-1}, see Fig. 2 E. The gas uptake rate r_{CO} increases by 30 % to 23.83 mmol L^{-1} h^{-1}, r_{H_2} and r_{CO_2} decrease by 42 % and 159 % to 21.50 mmol L^{-1} h^{-1} and -2.48 mmol L^{-1} h^{-1}, respectively, see Fig. 2 B. The biomass-specific ethanol formation decreases by 52 % to 0.71 mmol g^{-1} h^{-1}, while q_{AcOH} increases by 119 % to 3.09 mmol g^{-1} h^{-1}, see Fig. 2 C. The space-time yield of acetic acid increases by 45 % to 7.64 mmol L^{-1} h^{-1}, STY_{EtOH} decreases by 68 % to 1.75 mmol L^{-1} h^{-1} and the total space-time yield of C_2 products decreases for the first time, by 13 % to 9.39 mmol L^{-1} h^{-1}, see Fig. 2 D. In addition, the second gas flow increase leads to a significant shift in the product ratio from 0.95 to 4.37: the concentration of acetic acid is thus more than four times higher than that of ethanol, see Fig. 2 F.

Influence of an increased dilution rate with activated cell retention

As already shown, by activating cell retention, cell density increases significantly, see interval CR compared to $\overline{CR}$ in Fig. 2 E. The supply of liquid nutrient medium ($D = 0.03\,\mathrm{h^{-1}}$) kept at a constant rate in this experiment could by now represent a limitation due to the increased cell density. Therefore, to investigate the influence of dilution rate on the fermentation process, the dilution rate is gradually increased in the following experiment from $D = 0.03\,\mathrm{h^{-1}}$ ($\mathrm{CR_{D=0.03}}$) to $D = 0.04\,\mathrm{h^{-1}}$ ($\mathrm{CR_{D=0.04}}$) and then to $D = 0.05\,\mathrm{h^{-1}}$ ($\mathrm{CR_{D=0.05}}$), see Fig. 4.

Increasing the dilution rate from $0.03\,\mathrm{h^{-1}}$ to $0.04\,\mathrm{h^{-1}}$, i.e., a reduction of the liquid retention time τ of 24 %, leads to a significant decrease in biomass-specific gas uptake rates: $q_{\mathrm{H_2}}$ decreases by 38 % to $3.67\,\mathrm{mmol\,g^{-1}\,h^{-1}}$, q_{CO} by 36 % to $1.34\,\mathrm{mmol\,g^{-1}\,h^{-1}}$ and $q_{\mathrm{CO_2}}$ by 33 % to $0.79\,\mathrm{mmol\,g^{-1}\,h^{-1}}$, see Fig. 4 A. The second increase in dilution rate from $0.04\,\mathrm{h^{-1}}$ to $0.05\,\mathrm{h^{-1}}$, i.e., a reduction of τ of 20 %, leads to a further, slight decrease in biomass-specific gas uptake rates: $q_{\mathrm{H_2}}$ drops by 6 % to $3.46\,\mathrm{mmol\,g^{-1}\,h^{-1}}$, q_{CO} by 7 % to $1.24\,\mathrm{mmol\,g^{-1}\,h^{-1}}$ and $q_{\mathrm{CO_2}}$ by 6 % to $0.74\,\mathrm{mmol\,g^{-1}\,h^{-1}}$. Cell density, on the other hand, increases with increasing dilution rate: by 29 % to $12.91\,\mathrm{g\,L^{-1}}$ and by 9 % to $14.11\,\mathrm{g\,L^{-1}}$ for $\mathrm{CR_{D=0.04}}$ and $\mathrm{CR_{D=0.05}}$, respectively, see Fig. 4 E. The gas uptake rates at $\mathrm{CR_{D=0.04}}$ decrease compared to $\mathrm{CR_{D=0.03}}$ by 19 %, 17 % and 13 % to $47.45\,\mathrm{mmol\,L^{-1}\,h^{-1}}$, $17.33\,\mathrm{mmol\,L^{-1}\,h^{-1}}$ and $10.24\,\mathrm{mmol\,L^{-1}\,h^{-1}}$ for H_2, CO and CO_2, respectively, see Fig. 4 B. A further increase in the dilution rate to $0.05\,\mathrm{h^{-1}}$ does not lead to a reduction in the gas uptake rates; instead, the gas uptake rates increase slightly by 3 %, 1 %, and 2 % to $48.86\,\mathrm{mmol\,L^{-1}\,h^{-1}}$, $17.52\,\mathrm{mmol\,L^{-1}\,h^{-1}}$ and $10.47\,\mathrm{mmol\,L^{-1}\,h^{-1}}$ for H_2, CO and CO_2, respectively.

The biomass-specific ethanol formation, see Fig. 4 C, decreases significantly by 54 % to $0.40\,\mathrm{mmol\,g^{-1}\,h^{-1}}$ in case of $\mathrm{CR_{D=0.04}}$ and increases slightly by 2.5 % to $0.41\,\mathrm{mmol\,g^{-1}\,h^{-1}}$ in case of $\mathrm{CR_{D=0.05}}$, while q_{AcOH} remains unchanged at $0.57\,\mathrm{mmol\,g^{-1}\,h^{-1}}$ for $\mathrm{CR_{D=0.04}}$ and decreases by 11 % to $0.51\,\mathrm{mmol\,g^{-1}\,h^{-1}}$ for $\mathrm{CR_{D=0.05}}$. Overall, as the dilution rate increases,

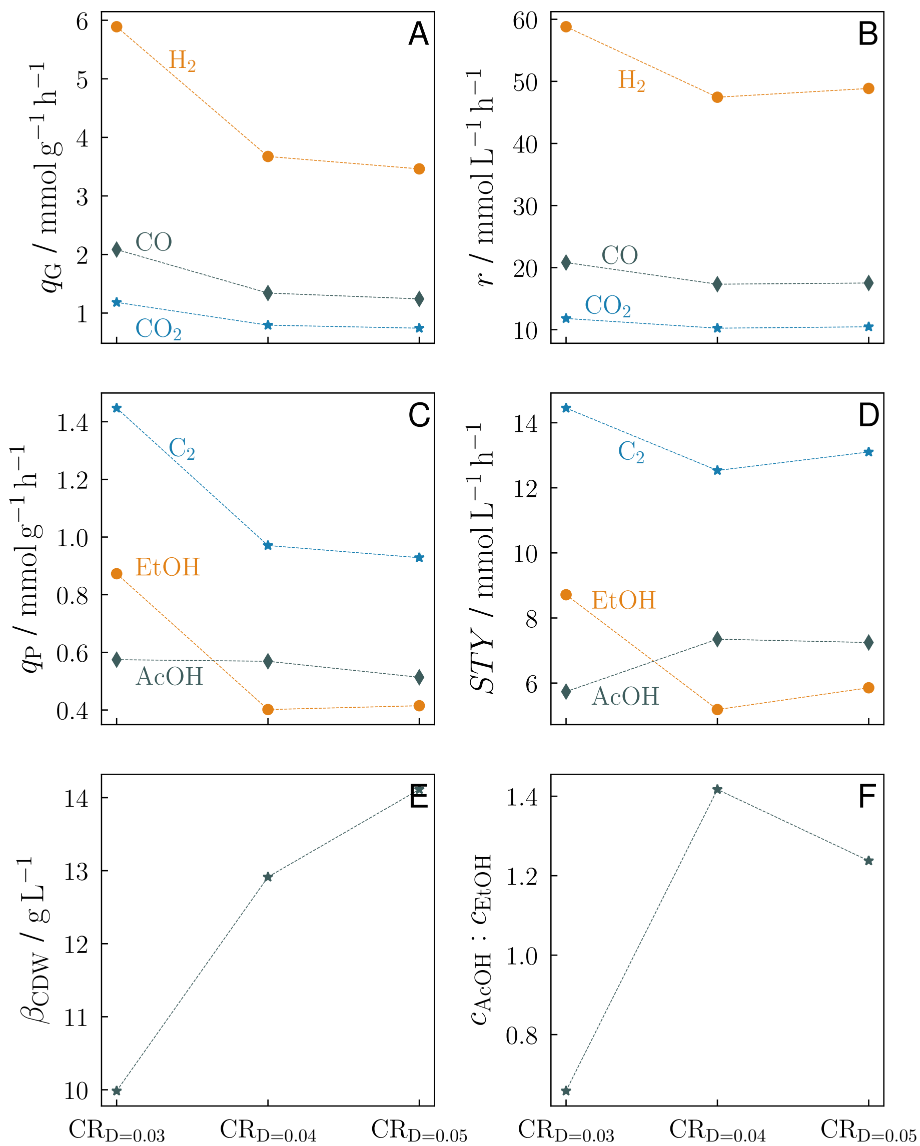

Figure 4: Increase of the dilution rate starting from $D = 0.03\,\mathrm{h}^{-1}$ ($\mathrm{CR_{D=0.03}}$) to $D = 0.04\,\mathrm{h}^{-1}$ ($\mathrm{CR_{D=0.04}}$) to $D = 0.05\,\mathrm{h}^{-1}$ ($\mathrm{CR_{D=0.05}}$). Averaged measured data of steady-state areas. A: biomass-specific gas consumption rate; B: gas consumption rate; C: biomass-specific productivity; D: space-time yield; E: concentration of cell dry weight; F: product ratio.

the sum of specific ethanol and acetic acid formation, $q_{\mathrm{C_2}}$, decreases by 33 % and 5 % to $0.97\,\mathrm{mmol\,g^{-1}\,h^{-1}}$ and $0.92\,\mathrm{mmol\,g^{-1}\,h^{-1}}$ for $\mathrm{CR_{D=0.04}}$ and $\mathrm{CR_{D=0.05}}$, respectively. The space-time yield of ethanol decreases by 40 % to $5.19\,\mathrm{mmol\,L^{-1}\,h^{-1}}$ after increasing the dilution rate to $0.04\,\mathrm{h}^{-1}$, while STY_{AcOH} increases by 28 % to $7.35\,\mathrm{mmol\,L^{-1}\,h^{-1}}$, see Fig. 4 D. A further increase of the dilution rate to $0.05\,\mathrm{h}^{-1}$ causes a slight increase in the space-time yield of ethanol by 13 % to 5.86 $\mathrm{mmol\,L^{-1}\,h^{-1}}$, while for acetic acid it remains almost constant at 7.25 $\mathrm{mmol\,L^{-1}\,h^{-1}}$ within the standard deviation. Overall, the space-time yield of acetic acid becomes larger than that of ethanol by increasing the dilution rate, thus the product ratio of acetic acid to ethanol reverses from 0.66 ($\mathrm{CR_{D=0.03}}$) to 1.42 ($\mathrm{CR_{D=0.04}}$) and 1.24 ($\mathrm{CR_{D=0.05}}$), respectively, see Fig. 4 F.

Deactivation of cell retention - reversibility

Microorganisms can change and adapt over long experimental runs. When evaluating measurement data, a distinction must therefore be made between the influence of parameter changes and the influence of adaptation processes on the fermentation process. To investigate whether the microorganisms have changed by switching on the external circuit for biomass retention, for example by adaptation, three intervals are considered: $\overline{CR}$, CR and $\overline{CR}_{\mathrm{B}}$. In the interval $\overline{CR}$, as a reference, the fermentation process is started without the operation of a biomass retention system, then the biomass retention system is activated in the interval CR (experiment A, for measurement data see Tab. S1). In another experiment B, biomass retention is deactivated from the on-going operation after 2700 h of operation with cell retention (interval $\overline{CR}_{\mathrm{B}}$, for measurement data see Tab. S2). If the microorganisms have changed due to the use of biomass retention, the measured values should differ significantly from those of the reference process $\overline{CR}$ after deactivation of cell retention.

By activating the biomass retention in the interval CR, the product ratio acetic acid to ethanol decreases from 2.33 to 0.81. After deactivation of biomass retention, this product ratio increases again significantly to 7.24; as in the interval $\overline{CR}$, more acetic acid is formed than ethanol. The cell densities of both intervals without biomass retention are similar: 1.19 $\mathrm{g\,L^{-1}}$ in the interval $\overline{CR}$ and 1.08 $\mathrm{g\,L^{-1}}$ in the interval $\overline{CR}_{\mathrm{B}}$. Furthermore, after deactivation of biomass retention ($\overline{CR}_{\mathrm{B}}$), there is a space-time yield of C_2 products of 5.67 ±0.24 $\mathrm{mmol\,L^{-1}\,h^{-1}}$ and is thus comparable to the space-time yield of the interval $\overline{CR}$ of 6.36 ±0.53 $\mathrm{mmol\,L^{-1}\,h^{-1}}$, taking into account the standard deviation. In addition, biomass retention leads to significantly reduced specific gas uptake rates: from $q_{\mathrm{CO+CO_2}} = 11.10\,\mathrm{mmol\,g^{-1}\,h^{-1}}$ without cell retention ($\overline{CR}$) to $5.48\,\mathrm{mmol\,g^{-1}\,h^{-1}}$ with cell retention (CR) and from $q_{\mathrm{H_2}} = 14.16\,\mathrm{mmol\,g^{-1}\,h^{-1}}$ without cell retention ($\overline{CR}$) to $9.54\,\mathrm{mmol\,g^{-1}\,h^{-1}}$ with cell retention (CR). After deactivation of biomass retention in the interval $\overline{CR}_{\mathrm{B}}$, again, specific gas uptake rates increase to $q_{\mathrm{CO+CO_2}} = 11.80\,\mathrm{mmol\,g^{-1}\,h^{-1}}$ and $q_{\mathrm{H_2}} = 17.60\,\mathrm{mmol\,g^{-1}\,h^{-1}}$ and are comparable to the specific gas uptake rates before activation of biomass retention ($\overline{CR}$).

Accumulation of carbon by using a total cell retention system

By using a total cell retention system with a pore size of the hollow fiber of $0.2\,\mu$m and by not using a bleed flow, an accumulation of carbon could occur in the reactor over time. Therefore, as part of another long-term experiment, a total of 23 samples were taken from the reactor over a period of 2000 h and the total carbon content of these non-centrifuged samples was determined by TOC analysis ($C_{\mathrm{total,measured}}$). Samples were then centrifuged and both cell density and product concentrations of ethanol and acetic acid were determined so that the carbon content of each product C_{CDW}, C_{AcOH}, and C_{EtOH} can be calculated. A value of 0.44 was assumed for the carbon mass fraction of the biomass.[27] The carbon fraction of the supplied nutrient medium C_{NM} was determined by TOC analysis. Then the ratio of the measured total carbon content to the sum of the individual carbon amounts can be calculated:

$$\Delta C = \frac{C_{\mathrm{total,measured}}}{C_{\mathrm{NM}} + C_{\mathrm{CDW}} + C_{\mathrm{AcOH}} + C_{\mathrm{EtOH}}} - 1 \tag{1}$$

Positive values of ΔC indicate that the measured total carbon content is greater than the sum of the recorded individual components, whereas the other way around is the case for negative values. Fig. 5 presents the values for ΔC over the duration of the experiment. The average is -6.63 percentage points and the median is -5.18 percentage points; consequently, the sum of the carbon from the culture medium, biomass, acetic acid and ethanol is greater than the total carbon measured. This is due to both measurement inaccuracies and simplifications made, such as assuming a carbon content of 0.44 of the biomass. If carbon were to accumulate, ΔC would have to increase and take positive values, but this is not evident in Fig. 5. Accumulation of carbon in the fermentation broth due to the use of total cell retention can therefore be ruled out for our experimental setup.

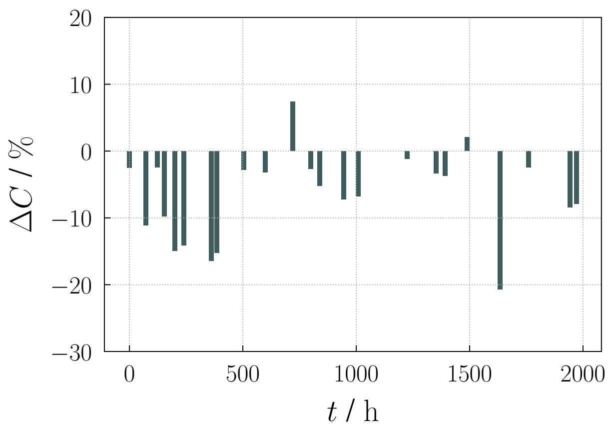

Figure 5: Relative difference between measured total carbon content and sum of calculated individual carbon contents over time with total cell retention.

Discussion

The experimental measurement results have shown that the use of a total biomass retention system increases the cell density by a factor of 2.6, while the total space-time yield is increased by a factor of 1.5. In addition, the product ratio reverses: without cell retention, more acetic acid is formed compared to ethanol, and with the use of a biomass retention system, more ethanol is formed compared to acetic acid. These observations are in contrast to the hypothesis established before the start of the experiments that cell retention would lead to an increase in cell density, but also to an increase in space-time yield proportional to cell density and to a product ratio that would remain constant. A shift in the product ratio due to adaptation of the microorganisms during operation of a biomass retention system is unlikely based on the measured data, see section *Deactivation of cell retention - reversibility*.

Rather, another regulatory mechanism might have been responsible for the product shift. Therefore, in this section, three possible reasons that could lead to a product shift and to a decrease in biomass-specific product formation are discussed: (1.) Limitation of substrate gas and nutrients, (2.) Reduced biomass-specific partial pressure of CO and (3.) Growth stagnation. Furthermore, it is discussed why the use of a total cell retention system does not lead to a steadily increasing cell density but to a biomass concentration with steady-state areas in all performed experiments.

Limitation of substrate gas and nutrients

At high cell densities, substrate gases could be limited. However, the gas flow increase has shown that the biomass-specific gas uptake rates increase for all gases, including CO, but not linearly with the gas flow increase. A further, second gas increase led to a decrease in cell density, reduced conversion of CO and, for the first time, net CO_2 production. We therefore conclude that although gas limitation was present prior to the gas flow increase at high cell densities, this was not responsible for the greatly reduced biomass-specific gas uptake rates, particularly for CO. However, reduced viability could be a possible cause, e.g. triggered by the peristaltic pump in the external circuit for biomass retention or by the absence of gas supply in this circuit. Therefore, determining viability could be important for future studies.

High cell densities with a constant supply of liquid nutrient medium can lead to limitations of individual nutrients.[28] The measured data on the effect of dilution rate, see Fig. 4, show a significant increase in cell density of 29 % after increasing the dilution rate from $D = 0.03\,\mathrm{h}^{-1}$ to $D = 0.04\,\mathrm{h}^{-1}$. This indicates a limitation of cell growth at a dilution rate of $0.03\,\mathrm{h}^{-1}$. Furthermore, the product ratio reverses, the molar fraction of ethanol after increasing the dilution rate is 0.41 instead of 0.6 before, and that of acetic acid is 0.59 instead of 0.4 before, see Fig. 6 $\mathrm{CR}_{\mathrm{D=0.03}}$ and $\mathrm{CR}_{\mathrm{D=0.04}}$.

Richter et al.[29] have shown by proteomic analysis that a lack of sulfur supply in terms of cysteine leads to reduced growth and the resulting excess of reduction potential leads to

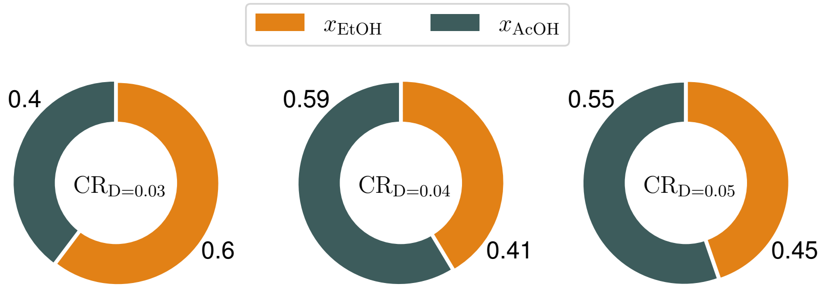

Figure 6: Mole fraction of ethanol (x_{EtOH}) and acetic acid (x_{AcOH}) of the product stream for three different dilution rates ($0.03\,\mathrm{h}^{-1}$, $0.04\,\mathrm{h}^{-1}$, $0.05\,\mathrm{h}^{-1}$) with activated cell retention (CR).

increased ethanol formation. Gaddy et al.[16] have described in their patent the possibility of a reduction of calcium pantothenate and cobalt in the culture medium to slow down both the acetyl-CoA cycle relative to the carbonyl branch and the THF cycle rate. This also leads to increased reduction potential and eventually increased ethanol formation. Wan et al.[30] have observed reduced growth of *Clostridium carboxidivorans* during yeast extract limitation. In a study by Phillips et al.,[31] the product ratio of ethanol to acetic acid increased during phosphate limitation. Considering these experimental results, our measured data indicate that at a dilution rate of $D = 0.03\,\mathrm{h}^{-1}$ and activated cell retention, there is a limitation of biomass growth caused by the nutrient medium, resulting in an excess of reduction potential that is converted to ethanol. In contrast, a further increase in the dilution rate to $0.05\,\mathrm{h}^{-1}$ leads just to a slight increase in cell density and to no significant change in the product ratio, see Fig. 6 $\mathrm{CR}_{\mathrm{D}=0.05}$. It can be concluded that there is sufficient nutrient supply to the microorganisms already at a dilution rate of $D = 0.04\,\mathrm{h}^{-1}$. Further increasing the dilution rate, contrary to the assumption of Richter et al.,[19] does not lead to an increase in product formation.

The experimental investigations on the influence of cell retention ($\overline{\mathrm{CR}}$ vs. CR, see Fig. 2 and Tab. S1) were performed at a constant dilution rate of $D = 0.03\,\mathrm{h}^{-1}$. Based on the above findings on the influence of the dilution rate, it must therefore be assumed that there was a limitation due to the nutrient medium after activation of the biomass retention. For this reason, the influence of this limiting effect on the measurement results will be discussed in the following. Activation of the biomass retention leads to increased biomass and to a reduced product ratio of acetic acid to ethanol from 2.33 to 0.81, and ethanol formation is thus favored at high cell densities (experiment A). Increasing the dilution rate in order to overcome the limitation of the nutrient medium leads to an increase of the product ratio from initially 0.66 ($CR_{D=0.03}$) to 1.42 ($CR_{D=0.04}$) (experiment B). Thus, more acetic acid is again formed than ethanol, but this surplus of 42 % is significantly smaller compared to 133 % without cell retention. Furthermore, the biomass-specific productivities q_{AcOH} and q_{EtOH} decrease significantly with the use of biomass retention and do not increase again by increasing the dilution rate. Therefore, it is unlikely that limitation by the nutrient medium when biomass retention is used is the only reason for the significant shift in the product ratio and for the decrease in biomass-specific productivities.

Partial pressure of CO in the off-gas as well as cell density are crucial influencing parameters

As already shown, the operation of a biomass retention system increases the cell density from initially 1.19 g L^{-1} and 1.08 g L^{-1} to an average value of 3.13 g L^{-1} (experiment A) and 12.33 g L^{-1} (experiment B), respectively. Fig. 7 shows all measured data from experiments A and B, where both CO and CO_2 were taken up simultaneously. It is clear that as the biomass-specific partial pressure of CO in the off-gas increases, the product ratio of acetic acid to ethanol increases proportionally, and the trend can be approximated by the following linear fit:

$$c_{\mathrm{AcOH}} : c_{\mathrm{EtOH}} = 0.3531 \, \frac{g_{\mathrm{CDW}}}{\mathrm{mbar}} \cdot \frac{p_{\mathrm{CO,off}}}{m_{\mathrm{CDW}}} + 0.2569 \qquad and\ R^2 = 0.9424 \tag{2}$$

It is remarkable that all measurement points sampled with a cell retention system are in the range of low biomass-specific partial pressures of CO ($< 3\,\mathrm{mbar}\,g_{\mathrm{CDW}}^{-1}$), whereas the measurement points without cell retention are assigned to significantly higher biomass-specific partial

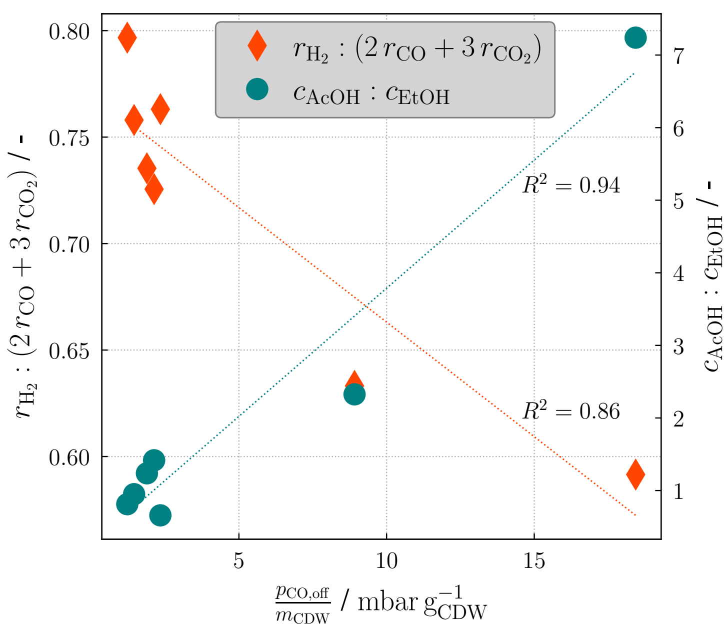

Figure 7: Hydrogen uptake ratio and product ratio as a function of biomass-specific CO partial pressure in the off-gas. The hydrogen uptake ratio takes into account that twice the molar amount of hydrogen is required for the complete conversion of CO to ethanol and three times the molar amount of hydrogen is required for the complete conversion of CO_2 to ethanol. This ratio is valid for data containing positive gas uptake rates. In addition to the measured points, linear fit of product ratio and hydrogen uptake ratio are shown.

pressures of CO ($8.91\,\mathrm{mbar}\,\mathrm{g}_{\mathrm{CDW}}^{-1}$ from experiment A in the interval $\overline{\mathrm{CR}}$ and $18.43\,\mathrm{mbar}\,\mathrm{g}_{\mathrm{CDW}}^{-1}$ from experiment B in the interval $\overline{\mathrm{CR}}_{\mathrm{B}}$). However, there is no clear tendency for the partial pressure of CO in the exhaust gas to decrease with higher cell density: e.g., at a cell density of $1.08\,\mathrm{g}\,\mathrm{L}^{-1}$ in the interval $\overline{\mathrm{CR}}_{\mathrm{B}}$, the partial pressure of CO in the exhaust gas is 43.9 mbar, while at a higher cell density of $9.98\,\mathrm{g}\,\mathrm{L}^{-1}$ in the interval $\mathrm{CR}_{\mathrm{D=0.03}}$ the partial pressure of CO in the exhaust gas is not smaller, but even higher with 51.4 mbar. Furthermore, the measured data shown in Fig. 7 indicate that a high CO gas conversion alone does not necessarily lead to a low biomass-specific partial pressure of CO in the exhaust gas: for example, at a CO conversion of 0.9 (interval $\overline{\mathrm{CR}}$, see Tab. S1), the biomass-specific partial pressure of CO in the exhaust gas is $8.91\,\mathrm{mbar}\,\mathrm{g}_{\mathrm{CDW}}^{-1}$, while at a slightly lower CO conversion of 0.87 (interval $\mathrm{CR}_{\mathrm{D=0.04}}$, see Tab. S2), the biomass-specific partial pressure of CO in the off-gas is not higher, but significantly lower by 76 % at $2.13\,\mathrm{mbar}\,\mathrm{g}_{\mathrm{CDW}}^{-1}$. Of particular importance for the biomass-specific partial pressure of CO in the exhaust gas is therefore the cell density: only at high cell densities as realized in experiment A and B by the use of a biomass retention system, there are low biomass-specific partial pressures of CO in the off-gas as well as low product ratios of acetic acid to ethanol in the fermentation broth. In their studies, Valgepea et al. [32] have observed lower acetic acid to ethanol product ratios at higher cell densities, too, and they attribute this to the maintenance of ATP homeostasis at elevated concentrations of extracellular acetic acid. Mock et al. [33] have a similar explanation approach and attribute high ethanol concentrations as a consequence of high acetic acid concentrations, as this could increase the intracellular acetic acid concentration compared to the intracellular acetaldehyde concentration, thus promoting ethanol formation via the AOR. Mayer et al. [22] observed in their studies with the microorganism *C. aceticum* an inhibitory effect of acetic acid exceeding a concentration of $10\,\mathrm{g}\,\mathrm{L}^{-1}$, Kantzow et al. [18] for *Acetobacterium woodii* from $8-12\,\mathrm{g}\,\mathrm{L}^{-1}$. Moreover, an inhibitory effect of high acetic acid concentrations on the growth of microorganisms would explain the stagnation of cell growth despite total cell retention in experiments A and B. Thus, the decrease in biomass-specific productivity of acetic acid after activation of cell retention in Fig. 2 C would be explained by the fact that the decrease in biomass-specific productivity of acetic acid would counteract a further increase in intracellular acetic acid concentration. The graph in Fig. 8 would be in agreement with this as well: A significant increase in ethanol concentration to $5\,\mathrm{g\,L^{-1}}$ or more is not observed until acetic acid concentrations are at least $8\,\mathrm{g\,L^{-1}}$. Therefore, from Fig. 8, it becomes clear that high ethanol concentrations only occur at high acetic acid concentrations. This can usually be achieved only with high cell densities due to the limited biomass-specific productivity of the microorganisms. This is consistent with Valgepea et al.[32] and Mock et al..[33] According to their findings, high ethanol concentrations were a consequence of high acetic acid concentrations. In contrast to acetic acid, ethanol concentrations up to $15\,\mathrm{g\,L^{-1}}$ do not have an inhibitory effect on the growth of *C. ljungdahlii*.[34]

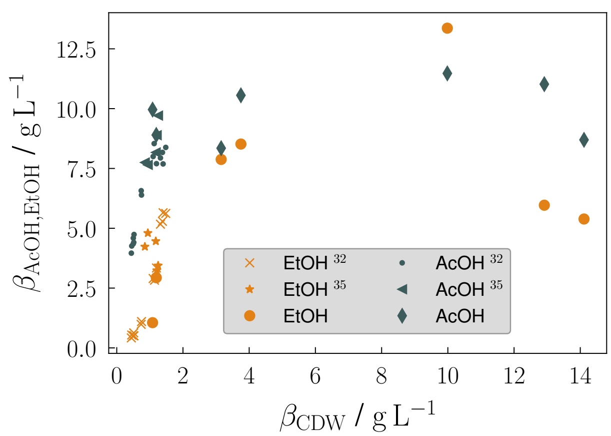

Figure 8: Product concentrations of acetic acid and ethanol as a function of cell density. Measured data of experiment A and B are compared with those from Stoll[35] (chemostat, $D = 0.03\,\mathrm{h^{-1}}$, *C. ljungdahlii* DSM 13528) and Valgepea et al.[32] (chemostat, $D = 0.04\,\mathrm{h^{-1}}$, *C. autoethanogenum* DSM 19630). Cell densities of $12.91\,\mathrm{g\,L^{-1}}$ and $14.11\,\mathrm{g\,L^{-1}}$ were obtained at higher dilution rates of $0.04\,\mathrm{h^{-1}}$ and $0.05\,\mathrm{h^{-1}}$. Adapted with permission from.[32] Copyright 2017 Elsevier Inc.

In addition, Valgepea et al.[32] found that with the increase in cell density, the ratio $q_{\mathrm{H_2}}/q_{\mathrm{CO}}$ decreased from 0.67 to 0.39, metabolic modeling demonstrated that the fraction of reduced ferredoxin generated by oxidation of CO to CO_2 increased by 19 %. In contrast, our measured data show that the ratio $q_{\mathrm{H_2}}/q_{\mathrm{CO}}$ increases from 1.29 to 2.13 when cell density is increased by activation of biomass retention. Therefore, it is likely that reduced ferredoxin was increasingly formed by hydrogen uptake and hydrogenase activity. Accordingly, both CO and H_2 serve as reducing agents for ferredoxin. This is consistent with studies by Bertsch and Müller,[36] Liew et al.[37] and Schuchmann and Müller.[14]

In addition, a linear relationship between the hydrogen-specific gas uptake and the biomass-specific partial pressure of CO in the exhaust gas is shown in Fig. 7. The hydrogen-specific gas uptake takes into account that twice the molar amount of H_2 is required for the complete conversion of CO to ethanol, and three times the molar amount of H_2 is required for the complete conversion of CO_2. The hydrogen-specific gas uptake therefore represents a stoichiometric ratio. The course of this ratio as a function of the biomass-specific partial pressure of CO in the exhaust gas can be approximated by the following linear fit:

$$r^*_{\mathrm{H_2}} = -0.0108\,\frac{g_{\mathrm{CDW}}}{\mathrm{mbar}} \cdot \frac{p_{\mathrm{CO,off}}}{m_{\mathrm{CDW}}} + 0.7707 \qquad \textit{and } R^2 = 0.8598 \tag{3}$$

From Fig. 7, it can be seen that at low biomass-specific partial pressures of CO in the off-gas, the specific hydrogen uptake is high, while at large biomass-specific CO partial pressures, it is low. This relationship can be explained by the inhibitory effect of CO on hydrogenase. The CO-induced inhibition of hydrogenase has already been investigated in various studies, see.[22,38–40] For example, Bertsch and Müller[36] were able to observe hydrogen uptake only above a conversion of CO of 90 %. We also see from our measurement data that after a gas flow increase (interval $\mathrm{CR}_{\dot{V}_{\mathrm{G}\uparrow\uparrow}}$ see Fig. 2), which resulted in a decrease of CO conversion to 84 %, the biomass-specific hydrogen uptake rate decreases significantly by 13 % from 9.96 mmol g^{-1} h^{-1} to 8.68 mmol g^{-1} h^{-1}. Therefore, taking into account the studies mentioned previously, it is likely that the second gas flow increase resulted in an increase in CO-induced inhibition of hydrogenase.

In addition, the product ratio of acetic acid to ethanol decreases with an increase in specific hydrogen uptake, see Fig. 7. This could be a result of excess reduction potential in the form of reduced ferredoxin and NADP due to increased activity of electron-bifurcating hydrogenase (Hyt). This excess can be reduced by the formation of ethanol via aldehyde ferredoxin oxidoreductase (AOR) or bifunctional acetaldehyde/alcohol dehydrogenase (AdhE), with AOR being the thermodynamically more favorable pathway.[33,36,41]

Redirection of reducing equivalents as a consequence of growth stagnation

Despite total cell retention in the intervals CR, $\mathrm{CR}_{\dot{V}_{\mathrm{G}\uparrow}}$ and $\mathrm{CR}_{\dot{V}_{\mathrm{G}\uparrow\uparrow}}$ in experiment A and $\mathrm{CR}_{\mathrm{D}=0.03}$, $\mathrm{CR}_{\mathrm{D}=0.04}$, and $\mathrm{CR}_{\mathrm{D}=0.05}$ in experiment B, there has not been a continuous increase in cell density; instead, constant cell densities have occurred in the intervals. Therefore, in the following discussion, we assume that cell retention, together with the other process conditions, led to a stagnation of cell growth.

With cell retention, the energy efficiency increases from 80 % to 89 %, see Tab. 3. The reason for the increased energy efficiency may be the reduced energy requirement of the microorganisms due to stagnation of cell growth, requiring only energy for maintenance metabolism.

Table 3: Energy efficiency of the process without cell retention ($\overline{\mathrm{CR}}$) and with cell retention (CR). The energy efficiency is calculated by the lower heating value of products ($\Delta H_{\mathrm{LHV}_{\mathrm{AcOH}}} = 869.4\,\mathrm{kJ\,mol^{-1}}$,[42] $\Delta H_{\mathrm{LHV}_{\mathrm{EtOH}}} = 1242\,\mathrm{kJ\,mol^{-1}}$[43]) divided by the lower heating value of reactants ($\Delta H_{\mathrm{LHV}_{\mathrm{H_2}}} = 241.84\,\mathrm{kJ\,mol^{-1}}$,[43] $\Delta H_{\mathrm{LHV}_{\mathrm{CO}}} = 282.99\,\mathrm{kJ\,mol^{-1}}$[43]). Idea of LHV-calculation is based on Köpke and Simpson.[44]

Interval	Measured substrate uptake and product formation in $\mathrm{mmol\,h^{-1}}$	Energy efficiency
$\overline{\mathrm{CR}}$	$37.2\,\mathrm{H_2} + 28.81\,\mathrm{CO} + 0.38\,\mathrm{CO_2} \longrightarrow 9.79\,\mathrm{AcOH} + 4.21\,\mathrm{EtOH}$	80 %
CR	$66.20\,\mathrm{H_2} + 31.10\,\mathrm{CO} + 6.97\,\mathrm{CO_2} \longrightarrow 9.18\,\mathrm{AcOH} + 11.30\,\mathrm{EtOH}$	89 %

In operation without cell retention, 80 % of ΔH_{LHV} taken up is captured in the products ethanol and acetic acid. It is now assumed that the remaining 20 %, i.e., the difference between the heating value of the reactant stream ($\sum \Delta H_{\mathrm{LHV_E}} \cdot \dot{n}_{\mathrm{E}}$) and the heating value of the product stream ($\sum \Delta H_{\mathrm{LHV_P}} \cdot \dot{n}_{\mathrm{P}}$), are necessary for the growth ($\beta_{\mathrm{CDW}} \cdot V_{\mathrm{W}} \cdot D \cdot e_{\mathrm{B}}$) and the maintenance metabolism ($\beta_{\mathrm{CDW}} \cdot V_{\mathrm{W}} \cdot p_{\mathrm{M}}$) of the microorganisms. Here, β_{CDW} represents the biomass concentration, V_{W} the working volume, D the dilution rate, e_{B} the specific energy to synthesize biomass and p_{M} represents the specific power for the maintenance metabolism:

$$\sum^{\overline{\mathrm{CR}}} \Delta H_{\mathrm{LHV_E}} \cdot \dot{n}_{\mathrm{E}} - \sum^{\overline{\mathrm{CR}}} \Delta H_{\mathrm{LHV_P}} \cdot \dot{n}_{\mathrm{P}} = \beta_{\mathrm{CDW}} \cdot V_{\mathrm{W}} \cdot D \cdot e_{\mathrm{B}} + \beta_{\mathrm{CDW}} \cdot V_{\mathrm{W}} \cdot p_{\mathrm{M}} \tag{4}$$

With the operation of cell retention, the term describing the specific energy to synthesize biomass can be neglected due to growth stagnation, thus Eq. 4 is simplified:

$$\sum^{\mathrm{CR}} \Delta H_{\mathrm{LHV_E}} \cdot \dot{n}_{\mathrm{E}} - \sum^{\mathrm{CR}} \Delta H_{\mathrm{LHV_P}} \cdot \dot{n}_{\mathrm{P}} = \beta_{\mathrm{CDW}} \cdot V_{\mathrm{W}} \cdot p_{\mathrm{M}} \tag{5}$$

Using Eq. 5, after inserting the values for heating value, biomass concentration and working volume, the necessary energy for maintenance metabolism $p_{\mathrm{M}} = 402.41\,\mathrm{J\,g^{-1}\,h^{-1}}$ is obtained. In comparison, for another organism, *Rhodospirillum rubrum*, Karmann et al.[45] reported a minimum supply necessary for maintenance metabolism of $0.2\,\mathrm{g_{CO}\,g_{CDW}^{-1}\,h^{-1}}$. Taking into account the lower heating value of CO, this results in a value for p_{M} of $2021\,\mathrm{J\,g^{-1}\,h^{-1}}$.

After inserting the value of $p_{\mathrm{M}} = 402.41\,\mathrm{J\,g^{-1}\,h^{-1}}$ together with the other values into Eq. 4, a value of $e_{\mathrm{B}} = 29.808\,\mathrm{kJ\,g^{-1}}$ is obtained for the amount of energy required to build up the biomass (for comparison: $\Delta H_{\mathrm{LHV_{Glucose}}} = 14.47\,\mathrm{kJ\,g^{-1}}$). As a comparison, if, on the other hand, the energy required to build up the biomass is estimated assuming an average biomass composition of $CH_{1.81}O_{0.52}N_{0.21}$ according to Villadsen et al.[46] and by the use of the method of calculating the lower heating value according to Grote et al.,[43] a value of $e_{\mathrm{B}} = 20.64\,\mathrm{kJ\,g^{-1}}$ is obtained.

At a dilution rate of $\mathrm{D} = 0.03\,\mathrm{h^{-1}}$ and with the experimentally determined amount of energy for biomass growth of $e_{\mathrm{B}} = 29.808\,\mathrm{kJ\,g^{-1}}$, a specific power for biomass synthesis of $p_{\mathrm{B}} = 894.24\,\mathrm{J\,g^{-1}\,h^{-1}}$ is calculated. Hence, the power to synthesize biomass p_{B} is twice as high as for maintenance metabolism $p_{\mathrm{M}} = 402.41\,\mathrm{J\,g^{-1}\,h^{-1}}$. Due to stagnation of cell growth triggered by the use of biomass retention, no buildup of new biomass occurs. As a consequence, energy is directed entirely to the less energy-intensive maintenance metabolism, which leads to the increase in energy efficiency calculated in Tab. 3.

Furthermore, 4.77 electrons per mole of biomass are required for the synthesis of biomass.[47] Therefore, for operation without cell retention in the interval $\overline{\mathrm{CR}}$, $6.81 \cdot 10^{-3}$ electrons per liter and hour are required for biomass buildup (at a dilution rate of $D = 0.03\,\mathrm{h}^{-1}$ and with $M_{\mathrm{CDW}} = 25.1\,\mathrm{g\,mol}^{-1}$[46]). If cell growth is stagnating, as in the interval CR due to the operation of a cell retention system, the electrons required to build up biomass are no longer needed. As a result, the electrons can be used elsewhere, e.g. for the reduction of acetic acid to ethanol, see Fig. 9, with the product ratio shifting towards ethanol. For this reason, in the following section, the influence on the product ratio will be estimated if in the interval $\overline{\mathrm{CR}}$, i.e., during operation without biomass retention, the electrons were used entirely for the reduction of acetic acid to ethanol and not for the synthesis of biomass.

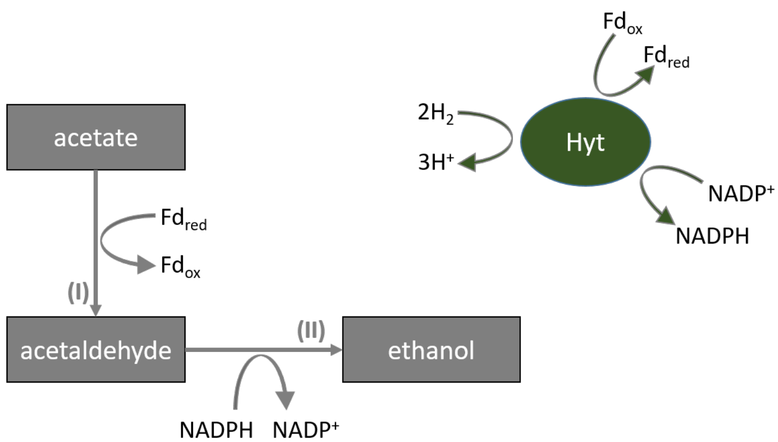

Figure 9: Reduction of acetate to ethanol in the WLP. Acetic acid is reduced to acetaldehyde via the AOR (I) and finally to ethanol via the AdhE (II). Four electrons are required for the reduction of acetate to ethanol, which can be provided, for example, via hydrogen uptake and electron-bifurcating hydrogenase (Hyt) with the carriers ferredoxin (Fd) and NADP.

Without cell retention, the product ratio of acetic acid to ethanol is 2.33. Eight electrons are required per mole of acetic acid, and 12 electrons are required per mole of ethanol, so by using the space-time yields from Tab. S1, the amount of electrons required can be calculated: $35.6 \cdot 10^{-3}$ electrons per liter and hour for acetic acid formation and $23 \cdot 10^{-3}$ electrons per liter and hour for ethanol formation. We now assume that the $6.81 \cdot 10^{-3}$ electrons per liter and hour initially required to build the biomass could be used to reduce acetic acid to ethanol. Four electrons are needed to reduce one mole of acetic acid to one mole of ethanol, see Fig. 9, thus $6.81 \cdot 10^{-3}/4 = 1.7$ millimoles of ethanol per liter and hour could be additionally built by reducing acetic acid to ethanol. Theoretically, this would increase the space-time yield for ethanol by $1.7\,\mathrm{mmol\,L^{-1}\,h^{-1}}$ to a total of $3.61\,\mathrm{mmol\,L^{-1}\,h^{-1}}$ and reduce it for acetic acid to $2.75\,\mathrm{mmol\,L^{-1}\,h^{-1}}$. Thus, the product ratio would decrease from initially 2.33 to 0.76, being comparable to the product ratio of 0.81 in the interval CR when operating a biomass retention system. This theoretical calculation demonstrates that the continuous synthesis of biomass during the operation of a CSTR without biomass retention is associated with considerable electron demand. The experimentally measured product shift towards the more reduced product ethanol when using a biomass retention system could be a consequence of the reduced electron demand of non-growing cells. This would be consistent with the results of Richter et al. [29] that excess reduction potential as a result of reduced cell growth is dissipated by increased ethanol formation via solventogenesis. In addition, studies by Liu et al. [48] in the context of a genome-scale model indicate ethanol formation as a consequence of excess reduction potential.

Conclusion

By using biomass retention with wild-type strain *Clostridium ljungdahlii* (DSM 13528), biomass increases significantly leading to an overall increase of the C_2 product titer to $24.83\,\mathrm{g\,L^{-1}}$ and to an increase of the C_2 space-time yield to $0.75\,\mathrm{g\,L^{-1}\,h^{-1}}$. Furthermore, space-time yield of ethanol with a value of $8.71\,\mathrm{mmol\,L^{-1}\,h^{-1}}$ becomes greater than the space-time yield of acetic acid, leading to a shift in the product ratio towards ethanol.

In addition, we found that the biomass-specific partial pressure of CO in the off-gas is an important tool for influencing hydrogen uptake and product ratio. Furthermore, we have shown that the continuous growth of the biocatalyst is associated with a high demand for electrons. The product shift towards ethanol at high cell densities through the usage of a biomass retention system is the result of an excess of reduction potential as a consequence of reduced or stagnated cell growth.

The measurement data from our long-term experiments of continuously operated fermentation both with and without biomass retention have therefore made an important contribution to identifying and characterizing the influencing factors that promote ethanol formation. By taking measurements in steady state, we have achieved to build up a valuable database for future kinetic modeling.

Symbols

β	$\mathrm{g\,L^{-1}}$	mass concentration of product i
c_i	$\mathrm{mmol\,L^{-1}}$	concentration of product i
ΔC	%	deviation of carbon content
D	$\mathrm{h^{-1}}$	dilution rate
e_B	$\mathrm{kJ\,g_{CDW}^{-1}}$	specific energy to synthesize biomass
ΔH_LHV	$\mathrm{kJ\,mol^{-1}}$	lower heating value
M	$\mathrm{g\,mol^{-1}}$	molar mass
m	g	mass
n	mmol	amount of substance
$\dot{n}$	$\mathrm{mmol\,min^{-1}}$	molar flow rate
P	W	power
p_i	mbar	partial pressure of component i
p_B	$\mathrm{J\,g_{CDW}^{-1}}\,h^{-1}$	specific power for the biomass synthesis
p_M	$\mathrm{J\,g_{CDW}^{-1}}\,h^{-1}$	specific power for the maintenance metabolism
q_G	$\mathrm{mmol\,g^{-1}\,h^{-1}}$	biomass-specific gas uptake rate
q_P	$\mathrm{mmol\,g^{-1}\,h^{-1}}$	biomass-specific productivity
R^2	-	coefficient of determination
r	$\mathrm{mmol\,L^{-1}\,h^{-1}}$	gas uptake rate
$r^*_\mathrm{H_2}$	-	gas uptake ratio of hydrogen to carbon
S	-	selectivity
STY	$\mathrm{mmol\,L^{-1}\,h^{-1}}$	space-time yield
T	°C	temperature
t	h	time
τ	h	liquid retention time
V	$\mathrm{m^3}$	volume
$\dot{V}$	$\mathrm{mL\,min^{-1}}$	volume flow
X_i	-	conversion of i
x_i	-	mole fraction

Abbreviation

AcOH	acetic acid
AdhE	bifunctional acetaldehyde/alcohol deydrogenase
AOR	aldehyde ferredoxin oxidoreductase
CDW	cell dry weight
CR	cell retention
$\overline{\text{CR}}$	without cell retention
CSTR	continuous stirred-tank reactor
EtOH	ethanol
Fd	ferredoxin
GC	gas chromatograph
HF	hollow fiber
HPLC	high performance liquid chromatography
Hyt	electron-bifurcating hydrogenases
IC	inorganic carbon
KOH	potassium hydroxide
NADP	nicotinamide adenine dinucleotide phosphate
NM	nutrient medium
PES	polyethersulfone
rpm	revolutions per minute
TC	total carbon
TOC	total organic carbon
vol.	volume
WLP	Wood-Ljungdahl pathway

Sub- and Superscripts

A	experiment A
B	experiment B
E	educt
G	gas
l	liquid
off	off-gas
P	product
W	working part

Author Contributions

L.P.: Conceptualization, methodology and execution of experiments. Analysis and evaluation of results. Writing of the manuscript. N.B.: significant input on concept and experimental design. Critical revision of the manuscript. J.S.: substantial input on concept, experimental design and evaluation of results. Critical revision of the manuscript; supervision.

Funding

The authors thank the Federal Ministry of Education and Research (BMBF) for financing the R&D program (Grant No. 03SFK2K0-2). We also gratefully acknowledge the funding of the Helmholtz Research Program "Materials and Technologies for the Energy Transition (MTET), Topic 3: Chemical Energy Carriers".

Acknowledgement

The authors thank E. Hauer for the contributions to the experimental work, K. Weiss and S. Henecka for the contributions to the mechanical work and V. Holderied and A. Lautenbach for the contributions to the analytical measurement.

Supporting Information Available

This information is available free of charge via the Internet at http://pubs.acs.org/.

- Complete experimental data (gas uptake rates, space-time yields and cell density) of experiment A and experiment B
- Detailed process flow diagram of the experimental test rig

References

(1) Tcvetkov, P.; Cherepovitsyn, A.; Fedoseev, S. The Changing Role of CO2 in the Transition to a Circular Economy: Review of Carbon Sequestration Projects. *Sustainability* **2019**, *11*, 5834.

(2) Pavan, M.; Reinmets, K.; Garg, S.; Mueller, A. P.; Marcellin, E.; Köpke, M.; Valgepea, K. Advances in systems metabolic engineering of autotrophic carbon oxide-fixing biocatalysts towards a circular economy. *Metab. Eng.* **2022**, *71*, 117–141.

(3) Perret, L.; Lacerda de Oliveira Campos, B.; Herrera Delgado, K.; Zevaco, T. A.; Neumann, A.; Sauer, J. CO x Fixation to Elementary Building Blocks: Anaerobic Syngas Fermentation vs. Chemical Catalysis. *Chem. Ing. Tech.* **2022**, *94*, 1667–1687.

(4) Dittrich, L.; Nohl, M.; Jaekel, E. E.; Foit, S.; de Haart, L.; Eichel, R.-A. High-Temperature Co-Electrolysis: A Versatile Method to Sustainably Produce Tailored Syngas Compositions. *J. Electrochem. Soc.* **2019**, *166*, F971–F975.

(5) Tang, D.; Tan, G.-L.; Li, G.-W.; Liang, J.-G.; Ahmad, S. M.; Bahadur, A.; Humayun, M.; Ullah, H.; Khan, A.; Bououdina, M. State-of-the-art hydrogen generation techniques and storage methods: A critical review. *J. Energy Storage* **2023**, *64*, 107196.

(6) Bolívar Caballero, J. J.; Zaini, I. N.; Yang, W. Reforming processes for syngas production: A mini-review on the current status, challenges, and prospects for biomass conversion to fuels. *Appl. Energy Combust. Sci.* **2022**, *10*, 100064.

(7) Singh, V.; Buelens, L. C.; Poelman, H.; Saeys, M.; Marin, G. B.; Galvita, V. V. Carbon monoxide production using a steel mill gas in a combined chemical looping process. *J. Energy Chem.* **2022**, *68*, 811–825.

(8) Leung, D. Y.; Caramanna, G.; Maroto-Valer, M. M. An overview of current status of carbon dioxide capture and storage technologies. *Renewable Sustainable Energy Rev.* **2014**, *39*, 426–443.

(9) Fernández-Blanco, C.; Veiga, M. C.; Kennes, C. Efficient production of n-caproate from syngas by a co-culture of Clostridium aceticum and Clostridium kluyveri. *J. Environ. Manage.* **2022**, *302*, 113992.

(10) Sun, X.; Atiyeh, H. K.; Huhnke, R. L.; Tanner, R. S. Syngas fermentation process development for production of biofuels and chemicals: A review. *Bioresour. Technol. Rep.* **2019**, *7*, 100279.

(11) Haas, T.; Krause, R.; Weber, R.; Demler, M.; Schmid, G. Technical photosynthesis involving CO2 electrolysis and fermentation. *Nat. Catal.* **2018**, *1*, 32–39.

(12) Fernández-Blanco, C.; Robles-Iglesias, R.; Naveira-Pazos, C.; Veiga, M. C.; Kennes, C. Production of biofuels from C1 -gases with Clostridium and related bacteria-Recent advances. *Microb. Biotechnol.* **2023**, *16*, 726–741.

(13) Wood, H. G. Life with CO or CO2 and H2 as a source of carbon and energy. *FASEB j.* **1991**, *5*, 156–163.

(14) Schuchmann, K.; Müller, V. Autotrophy at the thermodynamic limit of life: a model for energy conservation in acetogenic bacteria. *Nat. Rev. Microbiol.* **2014**, *12*, 809–821.

(15) Rosenbaum, F. P.; Müller, V. Energy conservation under extreme energy limitation: the role of cytochromes and quinones in acetogenic bacteria. *Extremophiles* **2021**, *25*, 413–424.

(16) Gaddy, J. L.; Arora, D. K.; Ko, C.-W.; Phillips, J. R.; Basu, R.; Wikstrom, C. V.; Clausen, E. C. Methods for increasing the production of ethanol from mibrobial fermentation. US 2003/0211585 A1, 2003.

(17) de Medeiros, E. M.; Posada, J. A.; Noorman, H.; Filho, R. M. Dynamic modeling of syngas fermentation in a continuous stirred-tank reactor: Multi-response parameter estimation and process optimization. *Biotechnol. Bioeng.* **2019**, *116*, 2473–2487.

(18) Kantzow, C.; Mayer, A.; Weuster-Botz, D. Continuous gas fermentation by Acetobacterium woodii in a submerged membrane reactor with full cell retention. *J. Biotechnol.* **2015**, *212*, 11–18.

(19) Richter, H.; Martin, M.; Angenent, L. A Two-Stage Continuous Fermentation System for Conversion of Syngas into Ethanol. *Energies* **2013**, *6*, 3987–4000.

(20) Phillips, J. R.; Klasson, K. T.; Clausen, E. C.; Gaddy, J. L. Biological production of ethanol from coal synthesis gas. *Appl. Biochem. Biotechnol.* **1993**, *39-40*, 559–571.

(21) Abubackar, H. N.; Veiga, M. C.; Kennes, C. Production of acids and alcohols from syngas in a two-stage continuous fermentation process. *Bioresour. Technol.* **2018**, *253*, 227–234.

(22) Mayer, A.; Schädler, T.; Trunz, S.; Stelzer, T.; Weuster-Botz, D. Carbon monoxide conversion with Clostridium aceticum. *Biotechnol. Bioeng.* **2018**, *115*, 2740–2750.

(23) Molitor, B.; Mishra, A.; Angenent, L. T. Power-to-protein: converting renewable electric power and carbon dioxide into single cell protein with a two-stage bioprocess. *Energy Environ. Sci.* **2019**, *12*, 3515–3521.

(24) Stoll, I. K.; Boukis, N.; Sauer, J. Syngas Fermentation at Elevated Pressure - Experimental Results. **2019**, 1255–1261.

(25) Routledge, S. J. Beyond de-foaming: the effects of antifoams on bioprocess productivity. *Comput. Struct. Biotechnol. J.* **2012**, *3*, 1–7.

(26) Oswald, F.; Dörsam, S.; Veith, N.; Zwick, M.; Neumann, A.; Ochsenreither, K.; Syldatk, C. Sequential Mixed Cultures: From Syngas to Malic Acid. *Front. Microbiol.* **2016**, *7*, 891.

(27) Infantes-López, A. Advancing towards biomass-derived syngas fermentation - Evaluation of process parameters and gas composition effects. Dissertation, Karlsruher Institut für Technologie, Karlsruhe, 2020.

(28) Kim, J.-H.; Lee, M.; Jeong, H.; Ko, S.; Moon, S.-H.; Chang, I. S. Recycling of minerals with acetate separation in biological syngas fermentation with an electrodialysis system. *Chem. Eng. J.* **2023**, *459*, 141555.

(29) Richter, H.; Molitor, B.; Wei, H.; Chen, W.; Aristilde, L.; Angenent, L. T. Ethanol production in syngas-fermenting Clostridium ljungdahlii is controlled by thermodynamics rather than by enzyme expression. *Energy Environ. Sci.* **2016**, *9*, 2392–2399.

(30) Wan, N.; Sathish, A.; Le You,; Tang, Y. J.; Wen, Z. Deciphering Clostridium metabolism and its responses to bioreactor mass transfer during syngas fermentation. *Sci. Rep.* **2017**, *7*, 10090.

(31) Phillips, J. R.; Atiyeh, H. K.; Tanner, R. S.; Torres, J. R.; Saxena, J.; Wilkins, M. R.; Huhnke, R. L. Butanol and hexanol production in Clostridium carboxidivorans syngas fermentation: Medium development and culture techniques. *Bioresour. Technol.* **2015**, *190*, 114–121.

(32) Valgepea, K.; de Souza Pinto Lemgruber, R.; Meaghan, K.; Palfreyman, R. W.; Abdalla, T.; Heijstra, B. D.; Behrendorff, J. B.; Tappel, R.; Köpke, M.; Simpson, S. D.; Nielsen, L. K.; Marcellin, E. Maintenance of ATP Homeostasis Triggers Metabolic Shifts in Gas-Fermenting Acetogens. *Cell Syst.* **2017**, *4*, 505–515.

(33) Mock, J.; Zheng, Y.; Mueller, A. P.; Ly, S.; Tran, L.; Segovia, S.; Nagaraju, S.; Köpke, M.; Dürre, P.; Thauer, R. K. Energy Conservation Associated with Ethanol Formation from H2 and CO2 in Clostridium autoethanogenum Involving Electron Bifurcation. *J. Bacteriol.* **2015**, *197*, 2965–2980.

(34) Ramió-Pujol, S.; Ganigué, R.; Bañeras, L.; Colprim, J. Effect of ethanol and butanol on autotrophic growth of model homoacetogens. *FEMS Microbiol. Lett.* **2018**, *365*, 1–4.

(35) Stoll, I. K. Einfluss eines erhöhten Prozessdrucks bei der Fermentation von Synthesegas: Charakterisierung der Druckfermentation im Rührkesselreaktor. Dissertation, Karlsruher Institut für Technologie, Karlsruhe, 2021.

(36) Bertsch, J.; Müller, V. Bioenergetic constraints for conversion of syngas to biofuels in acetogenic bacteria. *Biotechnol. Biofuels* **2015**, *8*, 210.

(37) Liew, F.; Martin, M. E.; Tappel, R. C.; Heijstra, B. D.; Mihalcea, C.; Köpke, M. Gas Fermentation-A Flexible Platform for Commercial Scale Production of Low-Carbon-Fuels and Chemicals from Waste and Renewable Feedstocks. *Front. Microbiol.* **2016**, *7*, 694.

(38) Jack, J.; Lo, J.; Maness, P.-C.; Ren, Z. J. Directing Clostridium ljungdahlii fermentation

products via hydrogen to carbon monoxide ratio in syngas. *Biomass Bioenergy* **2019**, *124*, 95–101.

(39) Ragsdale, S. W. Life with carbon monoxide. *Crit. Rev. Biochem. Mol. Biol.* **2004**, *39*, 165–195.

(40) Mohammadi, M.; Najafpour, G. D.; Younesi, H.; Lahijani, P.; Uzir, M. H.; Mohamed, A. R. Bioconversion of synthesis gas to second generation biofuels: A review. *Renewable Sustainable Energy Rev.* **2011**, *15*, 4255–4273.

(41) Perez, J. M.; Richter, H.; Loftus, S. E.; Angenent, L. T. Biocatalytic reduction of short-chain carboxylic acids into their corresponding alcohols with syngas fermentation. *Biotechnol. Bioeng.* **2013**, *110*, 1066–1077.

(42) Portz, H. *Brand- und Explosionsschutz von A - Z: Begriffserläuterungen und brandschutztechnische Kennwerte*, 1st ed.; Vieweg Praxis; Vieweg: Wiesbaden, 2005.

(43) Grote, K.-H.; Bender, B.; Göhlich, D. *Dubbel*; Springer Berlin Heidelberg: Berlin, Heidelberg, 2018.

(44) Köpke, M.; Simpson, S. D. Pollution to products: recycling of 'above ground' carbon by gas fermentation. *Curr. Opin. Biotechnol.* **2020**, *65*, 180–189.

(45) Karmann, S.; Panke, S.; Zinn, M. Fed-Batch Cultivations of Rhodospirillum rubrum Under Multiple Nutrient-Limited Growth Conditions on Syngas as a Novel Option to Produce Poly(3-Hydroxybutyrate) (PHB). *Front. Bioeng. Biotechnol.* **2019**, *7*, 59.

(46) Villadsen, J.; Nielsen, J.; Lidén, G. *Bioreaction engineering principles*, 3rd ed.; Springer: New York, NY and Heidelberg, 2011.

(47) Hermann, M.; Teleki, A.; Weitz, S.; Niess, A.; Freund, A.; Bengelsdorf, F. R.; Takors, R. Electron availability in CO2 , CO and H2 mixtures constrains flux distribution, energy

management and product formation in Clostridium ljungdahlii. *Microb. Biotechnol.* **2020**, *13*, 1831–1846.

(48) Liu, J. K.; Lloyd, C.; Al-Bassam, M. M.; Ebrahim, A.; Kim, J.-N.; Olson, C.; Aksenov, A.; Dorrestein, P.; Zengler, K. Predicting proteome allocation, overflow metabolism, and metal requirements in a model acetogen. *PLoS Comput. Biol.* **2019**, *15*, 1–16.

TOC Graphic